Effect of oxygen on the electronic band structure of II-O-VI alloys

W. Shan[*a], W. Walukiewicz[a], K.M. Yu[a], J.W. Ager III[a], J. Wu[a], J. Beeman[a], M.A. Scapulla[a,b], O.D. Dubon[a,b], E. E. Haller[a,b], Y. Nabetani[c], and P. Becla[d]
[a]Materials Sciences Division, Lawrence Berkeley National Laboratory, Berkeley, CA, 94720, USA;
[b]Dept. of Materials Science and Engineering, University of California, Berkeley, CA 94720, USA;
[c]Department of Electrical Engineering, University of Yamanashi, Kofu 400-8511, Japan;
[d]Department of Materials Science and Engineering, Massachusetts Institute of Technology, Cambridge, MA 02139, USA

ABSTRACT

We have studied the effects of composition and hydrostatic pressure on the direct optical transitions at the Γ point of the Brillouin zone in MBE-grown ZnO_xSe_{1-x} and ion-implantation-synthesized $Zn_{1-y}Mn_yO_xTe_{1-x}$ alloys. We observe a large O-induced band-gap reduction and a change in the pressure dependence of the fundamental band gap of the II-O-VI alloys. The effects are similar to those previously observed and extensively studied in highly mismatched III-N-V alloys. Our results are well explained in terms of the band anticrossing model that considers an anticrossing interaction between the highly localized oxygen states and the extended states of the conduction band of II-VI compounds. The O-induced modification of the conduction band structure offers an interesting possibility of using small amounts of O to engineer the optoelectronic properties of group II-O-VI alloys.

Keywords: Oxygen, ZnO_xSe_{1-x}, $Zn_{1-y}Mn_yO_xTe_{1-x}$, II-VI compounds, band-anticrossing, highly mismatched alloys, band structure, pressure effect, photovoltaic

1. INTRODUCTION

Highly mismatched semiconductor alloys (HMAs) in which a small fraction of constituent anion elements is replaced by elements with highly dissimilar properties have recently attracted considerable attention. The most extensively studied HMAs to date are III-N-V alloys. It has been found that the substitution of the group V element in group III-V compounds with small amounts of nitrogen leads to dramatic changes of the electronic properties. These include a reduction of the fundamental band-gap energy [1,2], a significant increase in electron effective mass and a decrease in electron mobility [3-5]. Furthermore a new optical transition (E_+) appears from the valence band to the conduction band at the Γ point [6,7]. As one quantitative example, the incorporation of only one percent of nitrogen into GaAs induces a strikingly large reduction of 0.18 eV in the fundamental band-gap energy [8].

These dramatic changes of the electronic properties have recently been explained accurately by a band anticrossing (BAC) model [6,9]. The anticrossing interaction between the extended conduction-band states of a semiconductor matrix and the highly localized electronic states introduced by the isoelectronic substitutional atoms with high electronegativity can be expressed as [6,9]

$$E_{\pm}(k) = \frac{1}{2}\left\{\left(E_M(k) + E_O\right) \pm \sqrt{\left(E_M(k) - E_O\right)^2 + 4V^2}\right\} \quad (1)$$

where $E_M(k)$ and E_O are, respectively, the energies of the unperturbed conduction band and of the localized states relative to the top of the valence band. The matrix element describing the interaction and hybridization between the localized states and the extended conduction-band states $V=C_{MO}x^{1/2}$, where C_{MO} is a constant describing the coupling between localized states and the extended states of the semiconductor matrix and x is the alloy composition.

* WShan@lbl.gov

Illustrated in Fig. 1 are schematic examples of the calculated band structure based on the BAC model. The interaction between the localized isoelectronic states and the extended conduction-band states has a pronounced effect on the dispersion relation of the two conduction subbands E_- and E_+. If the localized state is located within the conduction band of the matrix, as depicted in Fig.1(a), the conduction-band states at the E_- edge retain mostly the extended E_M-like character and those at the E_+ edge are more of localized and E_D-like character. If the localized states lie below the conduction-band edge, as displayed in Fig.1(b), the conduction-subband edges E_- and E_+ switch their characters: the E_- subband states assume the highly localized nature and E_+ subband states possess the character of extended state. It is clear from the figure that the energy positions of the subband edges E_- and E_+ given by Eq.(1) depend on alloy concentration x and the coupling parameter C_{MO}, as well as the location of E_O with respect to the conduction band edge E_M.

In this work, we review our recent research on a new group of HMAs based on II-VI compounds. We show that partial replacement of group-VI anions with more electronegative O atoms in II-VI compounds does have the effect similar to incorporating nitrogen into III-V materials. The ZnO_xSe_{1-x} and $Zn_{1-y}Mn_yO_xTe_{1-x}$ alloy systems are specifically chosen to represent the respective cases depicted in Fig.1. The observations of a significant band-gap reduction with increasing oxygen content in ZnO_xSe_{1-x} and two well-resolved spectral features associated with the E_- and E_+ band edges in $Zn_{1-y}Mn_yO_xTe_{1-x}$, as well as the classical band-anticrossing behavior in the pressure dependence of the fundamental band gaps of these samples can all be quantitatively explained by the anticrossing interaction between the extended states of the conduction band of the host matrix materials and the highly localized oxygen states located at the vicinity of the conduction-band edge.

2. EXPERIMENTAL

The ZnO_xSe_{1-x} samples used in this work were grown on GaAs (100) substrates by molecular beam epitaxy at a growth temperature of 350°C. Before the growth of ZnOSe epitaxial films, a 100-nm thick ZnSe buffer layer was deposited on the substrates. The O content in the alloy layers was controlled by varying the O_2 flow rate to a RF oxygen plasma source. The ZnOSe layer thickness is around 600 nm for all the samples. The oxygen concentration in the films was determined from Vegard's law using lattice constants determined from the double-crystal X-ray diffraction rocking

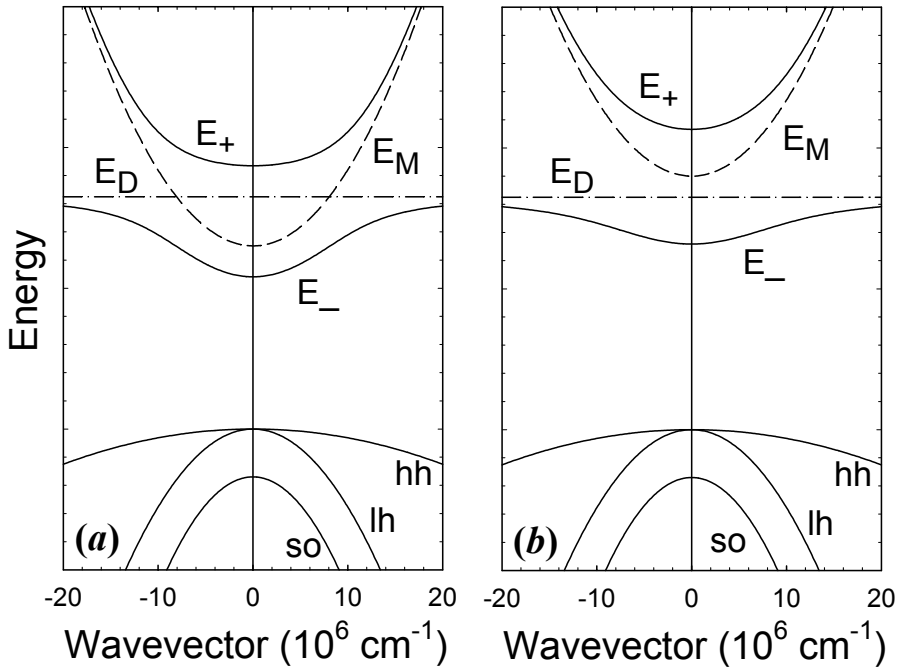

Fig.1. Illustration of the effects of band anticrossing on the Γ conduction band structure. (a) The highly electronegative isoelectronic impurity induced localized state resonant with the conduction band; (b) The localized state located below the conduction band. The solid lines are the restructured E_- and E_+ subbands resulting from the band anticrossing interaction between the localized states (dash-dotted line) and the extended states of the conduction band (broken line).

curves measured in the (400) and (511) planes [10]. The uncertainty in O concentration is about 20%.

The $Zn_{1-y}Mn_yO_xTe_{1-x}$ samples are synthesized using O ion implantation followed by pulsed laser melting (PLM). This approach is very effective in incorporating impurities into a crystal to levels well above the solubility limit due to the rapid recrystallization rate [11,12]. Synthesis of diluted GaN_xAs_{1-x} [13], as well as ferromagnetic $Ga_{1-x}Mn_xAs$ [14] using ion implantation and the PLM process have recently been demonstrated. Multiple energy implantation using 30 and 90 keV O^+ ions was carried out into $Zn_{0.88}Mn_{0.12}Te$ single crystals to form ~0.2 μm thick layers with the O concentration ranging from 0.0165 to 0.044. The reason for using ternary ZnMnTe as substrates is that the presence of Mn enhances and stabilizes the incorporation of O [15]. The O^+-implanted samples were pulsed-laser melted in air using a KrF laser (λ= 248 nm) with a pulse duration ~38ns. After passing through a multi-prism homogenizer, the fluence at the sample ranged between 0.020 and 0.3 J/cm^2.

Photo-modulated reflection (PR), photo-modulated transmission (PT) and photoluminescence (PL) measurements were carried out to measure the band gap energy of the ZnO_xSe_{1-x} and $Zn_{1-y}Mn_yO_xTe_{1-x}$ samples at room temperature (295 K). For the photo-modulation measurements, quasimonochromatic light from a Xenon arc or a tungsten halogen lamp dispersed by a 0.5-m monochromator was focused on the samples as a probe beam. A chopped HeCd laser beam (3250 or 4420 Å) provided the photomodulation. The PR or PT signals were detected by a Si photodiode using a phase-sensitive lock-in amplification system. For PL measurements, the 3250- Å HeCd laser line was used for excitation. Luminescence signals from the samples were dispersed by a 1-m double grating monochromator and detected by a photomultiplier tube. Application of hydrostatic pressure was accomplished by mounting small sample chips with sizes of ~200×200 μm^2 into gasketed diamond anvil cells.

3. RESULTS AND DISCUSSIONS

3.1 ZnO_xSe_{1-x}

Figure 2 shows PR spectra measured on the ZnO_xSe_{1-x} samples with different O content. In each case, the derivative-like spectral features correspond to the optical transitions from the valence-band edge to the conduction-band edge in the samples, and provide a direct measure of the band-gap energy. It is clear from Fig.2, the band gap of the samples shifts towards lower energy with increasing O concentration. The increasingly broadened PR spectral features are commonly observed in semiconductor alloys and can be partially attributed to the spatial alloy fluctuations of the O concentration in the sample.

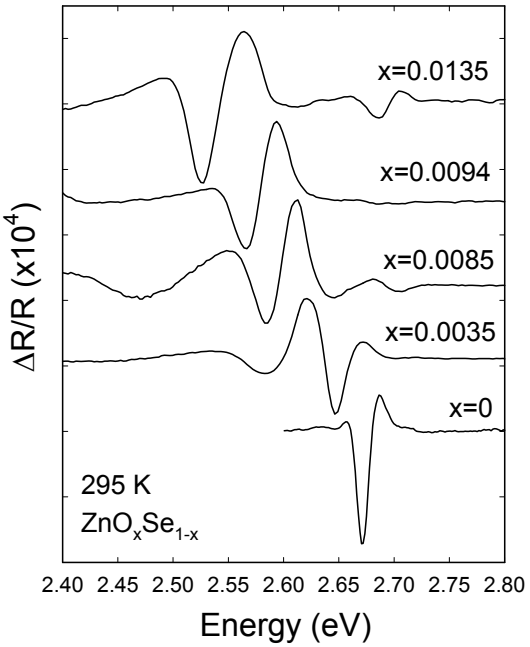

Fig. 2. PR spectra from ZnO_xSe_{1-x} at 295K.

Plotted in Fig. 3 are the band-gap energies of the ZnO_xSe_{1-x} samples as a function of O concentration. The energy gap for each sample was determined by fitting the corresponding PR spectral curve associated with the transition from the top of valence band to the bottom of the conduction band to the lineshape functional form of three-dimensional interband transitions [16,17]. The band gap decreases at a rate of about 0.1 eV per atomic percent of oxygen. This large O-induced band-gap reduction indicates a large band-gap bowing that bears a close resemblance to the analogous effects that have been extensively studied in GaN_xAs_{1-x} and $Ga_{1-y}In_yN_xAs_{1-x}$ HMAs (x<0.05). The solid line in the figure is the best fit using Eq.(1) to the experimental data with C_{MO} and E_O as adjustable parameters. The fit to the data is excellent. The large reduction of the fundamental band gap in ZnO_xSe_{1-x} with the increasing O

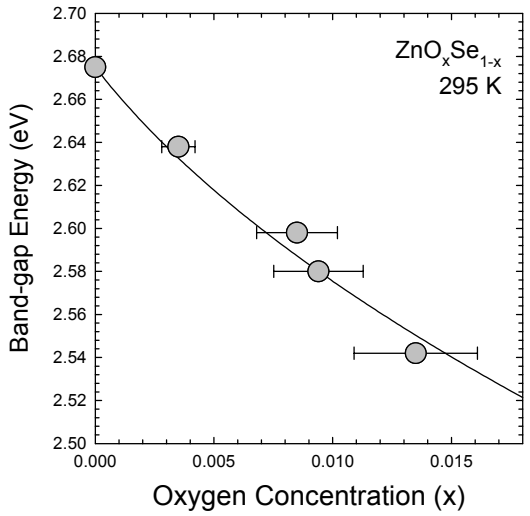

Fig. 3. Band-gap energies as a function of O concentration. The solid line is the best fit to the data using the BAC model.

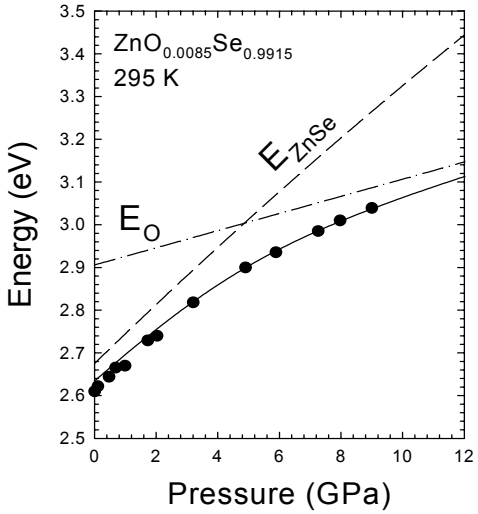

Fig. 4. The effect of pressure on PL transition energy associated with an x=0.0085 sample. The solid line is the calculated result using the BAC model.

concentration can be attributed to the downward shift of E_- relative to the valence band as a result of band anticrossing. The theoretical fitting results yield the energy position of O level E_O=E_V+2.90±0.02 eV and the interaction parameter C_{MO}=1.8±0.3 eV.

To further demonstrate that the band-gap reduction observed in the ZnO_xSe_{1-x} samples results from band anticrossing, we have used PL to measure the energy positions of the optical transitions associated with the fundamental band gap in a $ZnO_{0.0085}Se_{0.9915}$ sample as a function of applied hydrostatic pressure. The results are shown in Fig. 4, along with the known pressure dependence of PL features from thick ZnSe epilayers grown on GaAs substrates [18]. The pressure-induced energy shift of the optical transition related to the direct band gap of the sample is weaker and much more nonlinear than in ZnSe. This indicates that the application of high pressure gradually changes the character of the conduction-band edge (E_-) from extended-like to localized-like. The solid line in the figure shows the pressure dependence of the PL transition energy that corresponds to the change of the band gap of the sample calculated using Eq.(1) with the same values of E_O and C_{MO}.

It is very interesting to note that the energy position of O level in ZnSe determined here can be used to evaluate band-edge offsets between ZnTe and ZnSe. It has been well established that the energy levels of highly localized states are independent of the host material. For example, the locations of the d-states of transition metals, have been used to determine the band edge offsets [19] and the band-edge deformation potentials in compound semiconductors [20]. The O level was previously found to be located at about 0.24 eV below the conduction-band edge in ZnTe [21]. Combining this with current result of 0.22 eV above the conduction band edge of ZnSe for the O level, it yields a value of ΔE_C≈0.46 eV for the conduction-band offset and ΔE_V≈0.9 eV for the valence-band offset for ZnTe/ZnSe system.

The absence of spectral features related to the optical transition associated with the conduction-band edge E_+ in the ZnO_xSe_{1-x} samples used in this work is not inconsistent with the BAC model[6,9]. Note that the E_+ band edge has mostly localized-like character, and since the dipole interaction for optical transitions couples much more strongly to extended states than localized states, the transition related to E_+ is inherently weak. In addition, the energy separation between E_+ and E_- and the oscillator strength of the E_+ transition depend on the O content and the coupling parameter. In the case of GaN_xAs_{1-x}, with C_{MN}=2.7 eV, the E_+ transition can be spectrally observed only over the range of x > 0.005~0.008 [7,22,23]. This indicates that, with an almost two times smaller coupling parameter of C_{MO}≈1.8 eV in ZnO_xSe_{1-x}, it will certainly require an alloy composition of x>0.02 to resolve the E_+-transition related spectral feature.

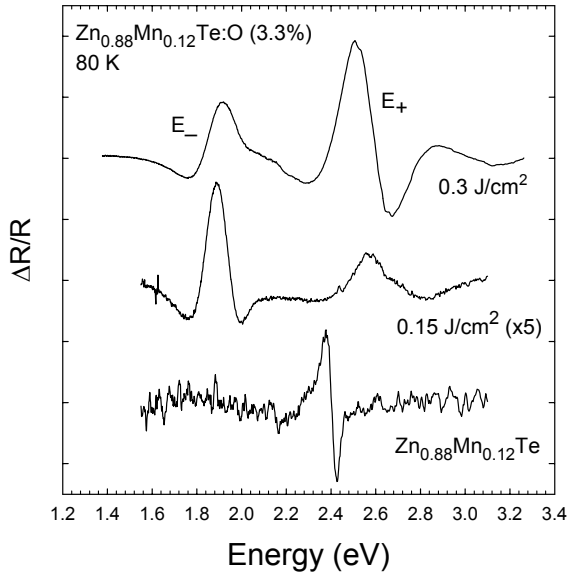

Fig. 5. PR spectra taken from $Zn_{0.88}Mn_{0.12}Te_{1-x}O_x$ samples at 80 K compared with the PR curve of $Zn_{0.88}Mn_{0.12}Te$ substrate.

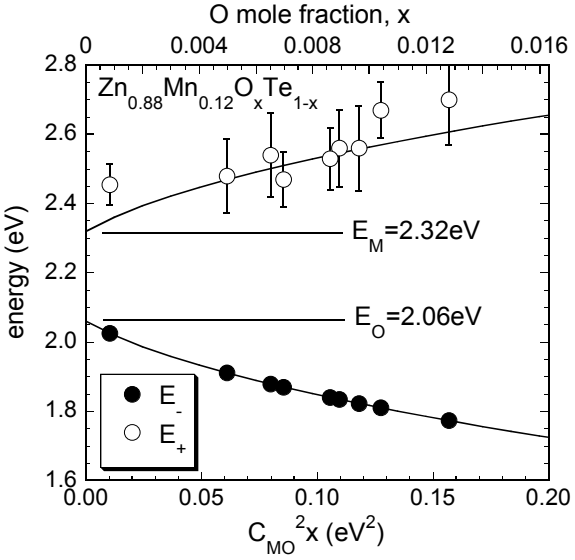

Fig. 6. The energy positions of E_- and E_+ for the $Zn_{0.88}Mn_{0.12}O_xTe_{1-x}$ alloys plotted against the O mole fractions x. The values of E_- and E_+ calculated according to the band anticrossing model are plotted as solid lines.

3.2 $Zn_{1-y}Mn_yO_xTe_{1-x}$

The relatively weak anticrossing interaction due to the relatively high location of the localized O level and small O mole fraction inhibits the observation of optical transitions associated with the E+ band edge in the currently available ZnO_xSe_{1-x} samples. To address the issue of E_+ transitions in II-O-VI alloys we have studied $Zn_{1-y}Mn_yO_xTe_{1-x}$ alloys. As discussed above, in the dilute limit ($x\rightarrow 0$) the O level is located below the conduction band of ZnTe. Because of a very small conduction band offset between ZnTe and ZnMnTe [24], the O level is expected to locate below the conduction band edge in ZnMnTe as well. Therefore, the E_- and E_+ band edges of $Zn_{1-y}Mn_yO_xTe_{1-x}$ formed by the band anticrossing interaction should possess a character opposite to that of ZnO_xSe_{1-x}, respectively, as described in Fig.1(b): E_- is of localized-like nature and E_+ is extended-like. The extended-like nature of the E_+ band edge of $Zn_{1-y}Mn_yO_xTe_{1-x}$ should have a relatively large oscillator strength to produce some detectable spectral response.

The PR spectra taken at 80 K from two $Zn_{0.88}Mn_{0.12}O_xTe_{1-x}$ samples implanted with 3.3% O^+ followed by PLM with a laser energy fluence of 0.15 and 0.3 J/cm^2 are shown in Fig. 5. The actual "active" O concentration (x) in the $Zn_{0.88}Mn_{0.12}O_xTe_{1-x}$ samples is estimated to be roughly around 1% by assuming a C_{MO}=3.5 eV[25]. However, it should be noted that the precise value of the composition x is not very important in the discussion presented here. A PR spectrum taken from the $Zn_{0.88}Mn_{0.12}Te$ used as the substrate in this work is also plotted in the figure for comparison. The derivative-like spectral feature of the PR curve of $Zn_{0.88}Mn_{0.12}Te$ corresponds to the optical transition from the valence-band edge to the conduction-band edge. The band-gap energy is found to be 2.40 eV at 80 K for the $Zn_{0.88}Mn_{0.12}Te$ matrix. For the oxygen containing samples, the PR spectra exhibit two features with energies distinctly different from the fundamental band gap of $Zn_{0.88}Mn_{0.12}Te$ matrix. These two features can be attributed to the transitions from the top of the valence band to the two conduction subband edges, E_- (~1.85 eV) and E_+ (~2.6 eV), formed by the band anticrossing interaction between the localized O states and the extended conduction-band states of the ZnMnTe matrix. The strong photomodulation signals of both E_- and E_+ indicate the extended nature of the electronic states in E_- and E_+ subbands.

The energy positions of E_- and E_+ for the $Zn_{0.88}Mn_{0.12}O_xTe_{1-x}$ alloys with different x are plotted in Fig. 6. The data were taken at room temperature from samples implanted with different amounts of O (1.65, 2.2 and 4.4%) and PLM processed with different energy fluences. The energy positions of the two transitions predicted by the BAC model are plotted as solid lines. Since, in this figure, the values of C_{MO}^2x were calculated from the energy of the E_- transition no error bars

are given for E_-. Given the broad linewidth of the PR feature corresponding to the E_+ transitions, the data in Fig.6 are in reasonable agreement with the calculations based on the BAC model.

The effects of applied pressure on the E_- transition in the $Zn_{0.88}Mn_{0.12}O_xTe_{1-x}$ samples were studied in order to verify the origin of the E_- band. The energy positions of the E_- transition in the sample treated by PLM with a laser energy fluence of 0.3 J/cm^2 has been measured as a function of applied hydrostatic pressure at room temperature. The results are shown in Fig. 7, along with the measured pressure dependence of the band gap of the $Zn_{0.88}Mn_{0.12}Te$ matrix. The room-temperature energy position of the E_+ transition at atmospheric pressure is also shown in the figure. The inset shows a typical PT spectrum recorded at high pressures. The broad PT feature on the lower energy side corresponds to the E_- transition and the narrow PT feature (E_g^{ZnMnTe}) on the higher energy side is the transition associated with the fundamental band gap of $Zn_{0.88}Mn_{0.12}Te$ substrate.

A linear fitting to the experimental data that are shown by open circles in Fig.7 yields the value of dE_g/dP=8.5 meV/kbar for the pressure dependence of the $Zn_{0.88}Mn_{0.12}Te$ band gap. The pressure-induced energy shift of the E_- transition is much weaker with an initial slope ≈ 2 meV/kbar than the pressure induced change of the direct band gap of $Zn_{0.88}Mn_{0.12}Te$ matrix. The weak pressure dependence of the E_- transition can be fully understood with the BAC model. The fact that E_- is located much closer to the energy level of the localized O states [Fig.1(b)] gives its wavefunction a pronounced O-like character. The solid lines through the experimental data in Fig. 7 are the calculated pressure dependencies of the E_- and E_+ transitions using Eq. (1). The best fits to the data yield the energy position of the O level (relative to the top of the valence band) $E_O=E_V+2.0\pm0.1$ eV at atmospheric pressure with a pressure dependence of 0.6±0.1 meV/kbar. It is clear from the figure that the pressure dependence of the E_- transition is slightly stronger than that of the O level as expected from the admixture of extended conduction-band Γ_C states of the matrix to the E_- band-edge states.

The present results have important inferences for the understanding of the origin of the unusual electronic structure of HMAs. They show very clearly that the BAC model provides a unifying description of the electronic structure of a large

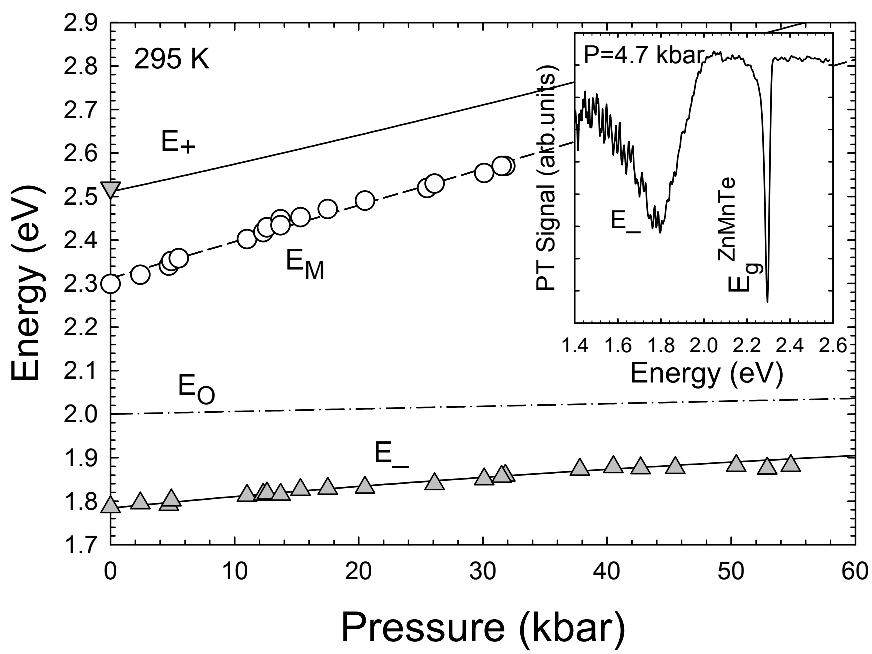

Fig. 7. Effect of pressure on the energy position of the E_ band edge of a $Zn_{0.88}Mn_{0.12}O_xTe_{1-x}$ sample (triangles). The change of the band gap of the $Zn_{0.88}Mn_{0.12}Te$ substrate with pressure is also displayed (open circles). The solid lines are theoretical fitting results. The dashed-dotted line is the location of E_O relative to the top of the valence band. The inset shows a typical PT spectrum of $Zn_{0.88}Mn_{0.12}O_xTe_{1-x}$ under pressure.

variety of different HMAs. They also provide strong arguments against other previously proposed models. It has been argued that the electronic structure of GaN_xAs_{1-x} alloys results from an interaction between the closely lying Γ_C, L_C, and X_C minima [26-28]. The interaction is caused by the perturbation potential resulting from the substitution of N atom on an As site. In these models the smaller and pressure-dependent pressure coefficient of the E_- transition observed in GaN_xAs_{1-x} alloys was attributed to the increasing contribution of the L_C and X_C minima whose pressure coefficients are much smaller than that of the Γ_C minimum. Apparently, these models cannot explain the results presented here. The large downward shift of 0.5 eV of the conduction band minimum (E_-) and the very weak pressure dependence of the band energy as shown in Fig.6 cannot be attributed to the influence from the conduction-band L and X edges because they are located far away from the Γ_C edge (>1.0 eV) in $Zn_{1-y}Mn_yTe$ [29]. Thus, our results directly confirm that the E_- transition together with the E_+ is the results of a band anticrossing interaction between the extended Γ conduction-band states and highly localized states in highly mismatched alloys.

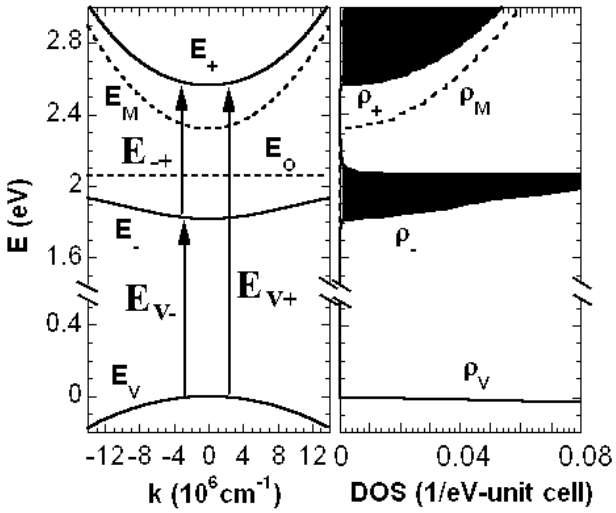

Fig. 8. The calculated energy band structure (left panel) and density of states (right panel) for $Zn_{0.88}Mn_{0.12}O_xTe_{1-x}$ with x~0.01. The three possible optical transitions are indicated in the left panel.

3.3 Photovoltaic application

The O-induced modification of the conduction band structure offers an interesting possibility of using small amounts of O to engineer the optoelectronic properties of group II-O-VI alloys. One of the many technological potentials of II-O-VI HMAs is for photovoltaic applications. Efforts to improve the efficiency of solar cells have led to extensive experimental and theoretical studies of new materials and cell designs. To date, the highest power conversion efficiency of ~33% has been achieved with multi-junction solar cells based on standard semiconductor materials [30-32]. It was recognized over thirty years ago that the introduction of states in a semiconductor band gap presents an alternative to multi-junction designs for improving the power conversion efficiency of solar cells [33-35]. It was argued that deep impurity or defect states could play the role of the intermediate states for this purpose. Detailed theoretical calculations indicate that a single junction cell with one or two properly located bands of intermediate states could achieve power conversion efficiencies up to 62% [34] and 71.7% [35], respectively. However, difficulties in controlling the incorporation of high concentrations of impurity or defect states have thwarted prior efforts to realize such materials.

With the multiple band gaps that fall within the solar energy spectrum, $Zn_{1-y}Mn_yO_xTe_{1-x}$ provides a unique opportunity for the realization of the proposed multiband solar cell. The energy band structure and the density of states for the case of $Zn_{0.88}Mn_{0.12}O_xTe_{1-x}$ alloy (with x~0.01) are shown in Fig. 8. An O derived narrow band of extended states E_- is separated from the upper subband E_+ by about 0.7 eV. Three types of optical transitions are possible in this band structure; (1) from the valence band to the E_+ subband, $E_{V+}=E_+(k=0)-E_V(k=0)=2.56$ eV, (2) from the valence band to E_- subband, $E_{V-}=E_-(k=0)-E_V(k=0)=1.83$ eV and (3) from E_- to E_+, $E_{+-}=E_+(k=0)-E_-(k=0)=0.73$ eV. These three absorption edges span much of the solar spectrum, indicating that these alloys could be good candidates for the multi-band semiconductors envisioned for high efficiency photovoltaic devices.

4. CONCLUSIONS

We have studied the effect of oxygen on the electronic band structure of ZnO_xSe_{1-x} and $Zn_{1-y}Mn_yO_xTe_{1-x}$ alloys by investigating the optical transitions associated with the Γ point at the conduction-band and the valence-band edges, as well as the dependence of the transitions on applied pressure. A number of classical band-anticrossing behaviors

resulting from the strong interaction between the localized O states and the extended conduction-band states of the host material matrix have been observed in the samples studied in this work: A significant band-gap reduction with increasing O concentration in ZnO_xSe_{1-x} samples, optical transitions related to two conduction subbands E_- and E_+ in $Zn_{1-y}Mn_yO_xTe_{1-x}$ samples, and the demonstration of characteristic band-anticrossing behavior in the pressure dependence of the fundamental band gap in both alloy systems. These experimental results confirm that replacing group-VI anions in II-VI materials with isoelectronic but more electronegative O atoms does form highly mismatched II-O-VI alloy systems. The O-induced modification of the conduction band structure can be well described using the band anticrossing model that has been successfully applied to the III-N-V alloys. The O-induced modification of the conduction band structure offers the interesting possibility of using small amounts of O to engineer the optoelectronic properties of group II-O-VI alloys.

ACKNOWLEDGEMENTS

This work is supported by the Director, Office of Science, Office of Basic Energy Sciences, Division of Materials Sciences and Engineering, of the U.S. Department of Energy under Contract No. DE-AC03-76SF00098.

REFERENCES

1. M. Weyers, M. Sato, and H. Ando, Jpn. J. Appl. Phys. **31**, L853(1992).
2. M. Kondow, K. Uomi, K. Hosomi and T. Mozume, Jpn. J. Appl. Phys. **33**, L1056(1994).
3. C. Skierbiszewski, P. Perlin, P. Wisniewski, W. Knap, T. Suski, W. Walukiewicz, W. Shan, K.M. Yu, J.W. Ager, E.E. Haller, J.F. Geisz, and J.M. Olson, Appl. Phys. Lett. **76**, 2409(2000).
4. J.F. Geisz, D.J. Friedman, J.M. Olson, S.R. Kurtz, and M.B. Keyes, J. Cryst. Growth, **195**, 401(1998).
5. S.R. Kurtz, Allerman, C.H. Seager, R.M. Sieg, and E.D. Jones, Appl. Phys. Lett. **77**, 400(2000).
6. W. Shan, W. Walukiewicz, J. W. Ager III, E. E. Haller, J. F. Geisz, D. J. Friedman, J. M. Olson, and S. R. Kurtz, Phys. Rev. Lett. **82**, 1221(1999).
7. J. D. Perkins, A. Masceranhas, Y. Zhang, J. F. Geisz, D. J. Friedman, J. M. Olson, and S. R. Kurtz, Phys. Rev. Lett. **82**, 3312(1999).
8. K. Uesugi, N. Marooka and I. Suemune, Appl. Phys. Lett. **74**, 1254 (1999).
9. W. Walukiewicz, W. Shan, J. W. Ager III, D. R. Chamberlin, E. E. Haller, J. F. Geisz, D. J. Friedman, J. M. Olson, and S. R. Kurtz, in *Photovoltaics for the 21st Century*, ed. V.K. Kapur, R.D. McDonnell, D. Carlson, G.P. Ceasar, and A. Rohatgi, (The Electrochemical Society, Pennington, NJ, 1999), p.199.
10. Y. Nabetani, T. Mukawa, Y. Ito, and T. Matsumoto, Appl. Phys. Lett. **83**, 1148(2003).
11. C. W. White and P. S. Peercy, *Laser and Electron Beam Processing of Materials* (Academic Press, New York, 1980).
12. S. Williams, in *Laser Annealing of Semiconductors*, eds. J. M. Poate and J. W. Mayer, (Academic Press, New York, 1982) p. 385.
13. K. M. Yu, W. Walukiewicz, M. A. Scarpulla, O. D. Dubon, J. Jasinski, Z. Liliental-Weber, J. Wu, J. W. Beeman, M. R. Pillai, and M. J. Aziz, J. Appl. Phys. **94**, 1043(2003).
14. M. A. Scarpulla, K.M. Yu, O. Monteiro, M. Pillai, M.C. Ridgway, M.J. Aziz, and O.D. Dubon, Appl. Phys. Lett. **82**, 1251(2003).
15. K. M. Yu, W. Walukiewicz, J. Wu, J. W. Beeman, J. W. Ager III, E. E. Haller, I. Miotkowski, A. K. Ramdas, and P. Becla, Appl. Phys. Lett. **80**, 1571(2002).
16. D. E. Aspnes, in *Optical Properties of Solid*, ed. M. Balkanski (North-Holland, Amsterdam, 1980), Chap. 4A.
17. O. J. Glembocki, SPIE Proc. Vol.**1286**, 2(1990).
18. J.A. Tuchman, S. Kim, Z.F. Sui, and I.P. Herman, Phys. Rev. B**46**, 13371(1992).
19. J. M. Langer and H. Heinrich, Phys. Rev. Lett, **55**, 1414(1985).
20. D. D. Nolte, W. Walukiewicz, and E. E. Haller, Phys. Rev. Lett, **59**, 501(1987).
21. W. Walukiewcz, W. Shan, K.M. Yu, J.W. Ager III, E.E. Haller, I. Miotkowski, M.J. Seong, H. Alawadhi, and A.K. Ramdas, Phys. Rev. Lett. **85**, 1552(2000).
22. W. Shan, W. Walukiewicz, J. W. Ager, E. E. Haller, J. F. Geisz, D. J. Friedman, J. M. Olson, and S. R. Kurtz, J. Appl. Phys. **86**, 2349(1999).
23. P.J. Klar, *et al*, Appl. Phys. Lett. **76**, 3439(2000).
24. K.M. Yu, W. Walukiewicz, J. Wu, J.W. Beeman, J.W. Ager III, E.E. Haller, I. Miotkowski, A.K. Ramadas, and P.

Becla, Appl. Phys. Lett. **80**, 1571(2002).
25. K. M. Yu, W. Walukiewicz, J. Wu, W. Shan, J. W. Beeman, M. A. Scarpulla, O. D. Dubon, and P. Becla, Phys. Rev. Lett. **91**, 246203(2003).
26. E.D. Jones, N.A. Modine, A.A. Allerman, S.R. Kurtz, A.F. Wright, S.T. Tozer, and X. Wei, Phys. Rev. B**60**, 4430(1999).
27. T. Mattila, S.H. Wei, and A. Zunger, Phys. Rev. B**60**, R11245(1999).
28. N.G. Szwacki and P. Boguslawski, Phys. Rev. B**64**, 16201R(2001).
29. *Landolt-Börnstein*, eds. O. Madelung and M. Schultz, New Series, Group 3, Vol.22, Part a, Springer-Verlag, Berlin, 1988.
30. P.K. Chiang, J.H. Ermer, W.T. Nishikawa, D.D. Krut, D.E. Joslin, J.W. Eldredge, B.T. Cavicchi, and J.M. Olson, Proc. 25th IEEE Photovoltaic Specialists Conf. (IEEE New York, 1996) p. 183.
31. S. R. Kurtz, D. Myers, and J. M Olson, Proc. 26th IEEE Photovoltaic Specialists Conf. (IEEE, New York, 1997) p. 875.
32. R. R. King, P. C. Colter, D. E. Joslin, K. M. Edmondson, D. D. Krut, N. H. Karam, and Sarah Kurtz, Proc. 29th IEEE Photovoltaic Specialists Conf. New Orleans, 2002 (IEEE, New York, 2002) p. 852.
33. M. Wolf, Proc. IRE, **48**, 1246(1960).
34. A. Luque and A. Marti, Phys. Rev. Lett. **78**, 5014(1997).
35. A. S. Brown, M. A. Green and R. P. Corkish, Physica, E**14**, 121(2002).
36. W. Shockley and H. J. Queisser, J. Appl. Phys. **32**, 510(1961).